Nano Research

Open Access

Research Article

Polymerization-with-assembly enables homogeneous circularly polarized luminescence structures

Mingjiang Zhang[1,§], Wenting Gao[1,2,§], Shanshan Zhao[1], and Taotao Zhuang[1] ✉

[1] *Division of Nanomaterials & Chemistry, Hefei National Research Center for Physical Sciences at the Microscale, Department of Chemistry, University of Science and Technology of China, Hefei 230026, China*
[2] *School of the Gifted Young, University of Science and Technology of China, Hefei 230026, China*
[§] *Mingjiang Zhang and Wenting Gao contributed equally to this work.*

Cite this article: *Nano Research*, **2025**, *18*, 94907150. https://doi.org/10.26599/NR.2025.94907150

ABSTRACT: Semiconductor quantum dots (QDs) with circularly polarized luminescence (CPL) characteristics hold significant promise for a range of applications, including information security, three-dimensional (3D) display, quantum computing, and spintronics. Recent approaches combining QDs with chiral liquid crystal assemblies have demonstrated amplified CPL performance (specifically, luminescence dissymmetry factor, g_{lum} > 10^{-1}). However, the inherent fluidity and alignment sensitivity of chiral liquid crystals, along with QD aggregation and phase separation, continue to hinder the uniformity and long-term stability of these systems. In this work, we developed an *in-situ* helical co-assembly polymerization strategy that covalently incorporated InP-based QDs into chiral liquid crystal polymer templates, forming QD-based polymeric superhelical structures. We synthesized high-quality InP/ZnSeS/ZnS QDs and functionalized their surfaces with polymerizable groups to enable reactivity. By precisely tuning the photonic bandgap of the chiral liquid crystal polymers, we achieved chiral parented templates with high chiroptical activity overlapping full-visible-spectrum. Through covalent crosslinking with the QDs, a polymer network was formed, resulting in a maximum g_{lum} of 1.0. This polymerization-with-assembly approach offers exceptionally flexible and precise control over both the composition and architecture of superhelical materials, paving the way for high-quality CPL materials with broad applications in advanced technologies.

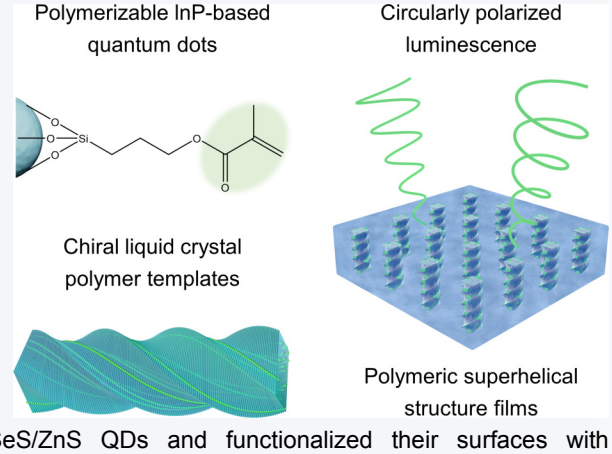

KEYWORDS: circular polarized luminescence, polymeric superhelical structure, quantum dots, chiral liquid crystal polymer

1 Introduction

Circularly polarized light, characterized by optical chirality and spin angular momentum, is of significance in fields such as quantum computing, information security, advanced displays, and spintronics [1–7]. Chiral luminescent materials can directly emit unequal amounts of left- and right-handed circularly polarized luminescence (CPL) under excitation, facilitating further integration of functional devices [8–10].

Semiconductor quantum dots (QDs)—known for their narrow emission spectra, enhanced stability, resistance to photobleaching, and high quantum yields—are well-suited for optoelectronic applications [11–13]. Among these, InP-based QDs have garnered significant attention due to their heavy metal-free composition, positioning them as ideal candidates for CPL systems [14]. Conventional methods for generating QD-based CPL materials typically involve synthesizing intrinsically chiral structures or modifying surface ligands. However, these methods generally result in low luminescence dissymmetry factor (g_{lum}) in the range between 10^{-4} and 10^{-2}, insufficient for practical applications [15–17].

Chiral liquid crystals (CLCs)—as quasi-one-dimensional photonic crystal materials—allow to self-assemble with luminescent materials for constructing highly ordered helical structures [18–22]. These structures can combine QDs to achieve amplified CPL with g_{lum} values over 10^{-1}, making CLCs ideal chiral templates for generating and amplifying CPL [23, 24]. However, CLCs possess inherent fluidity, requiring encapsulation in liquid crystal cells or polymers for practical applications [25]. Their alignment is also

Received: September 30, 2024; **Revised:** October 30, 2024
Accepted: November 25, 2024

✉Address correspondence to tzhuang@ustc.edu.cn

easily disrupted by external stimuli (electric, thermal, mechanical, or others) [26–28], suppressing CPL performance. Additionally, QDs tend to aggregate and phase-separate within the CLC matrix, compromising the long-term stability of CPL systems [29], while the polar environment is easy to quench the fluorescence of certain QDs, further limiting performance. Surface ligand engineering of QDs, by introducing polymerizable functional groups, can endow them with polymerization reactivity, enabling their stable dispersion and chemical bonding within polymerizable chiral liquid crystal templates, which offers a promising solution to these challenges [30].

Here, we report the design and synthesis of a series of CPL-active polymeric superhelical structures (PSS) based on InP QDs for the first time, using our designed *in-situ* helical co-assembly polymerization strategy. We synthesized high-quality, lead- and cadmium-free InP/ZnSeS/ZnS QDs, coating their surfaces with a thin SiO_2 layer and grafting polymerizable functional groups to impart reactive polymerization capabilities. By tuning the ratio of chiral dopants in the liquid crystal polymer matrix, we fabricated multicolored CLC polymer templates, achieving a maximum g_{lum} of 1.0 upon co-polymerization with the QDs. This work provides a novel approach for developing QD-based CPL materials, showing the promising in applications of information security, advanced displays, and spintronics, etc.

2 Results and discussion

To enable homogeneous circularly polarized luminescence structures, we proposed to synthesize surface-functionalized InP-based QDs to be assembled and polymerized with a CLC polymer template, enhancing the stability and dispersibility of the QDs within the system (Fig. 1(a)). Specifically, we synthesized high-quality InP/ZnSeS/ZnS QDs (Figs. S1 and S2 in the Electronic Supplementary Material (ESM)), and encapsulated them with a uniform SiO_2 layer through rapid hydrolysis of tetraethyl orthosilicate (TEOS) and tetramethyl orthosilicate (TMOS) in the presence of trace amounts of water in analytical-grade n-hexane [31]. The SiO_2 layer acts as an effective passivation, protecting the QDs from chemical degradation and enhancing their overall stability [32]. Moreover, this SiO_2 coating serves as a platform for subsequent surface-mediated functionalization. By further

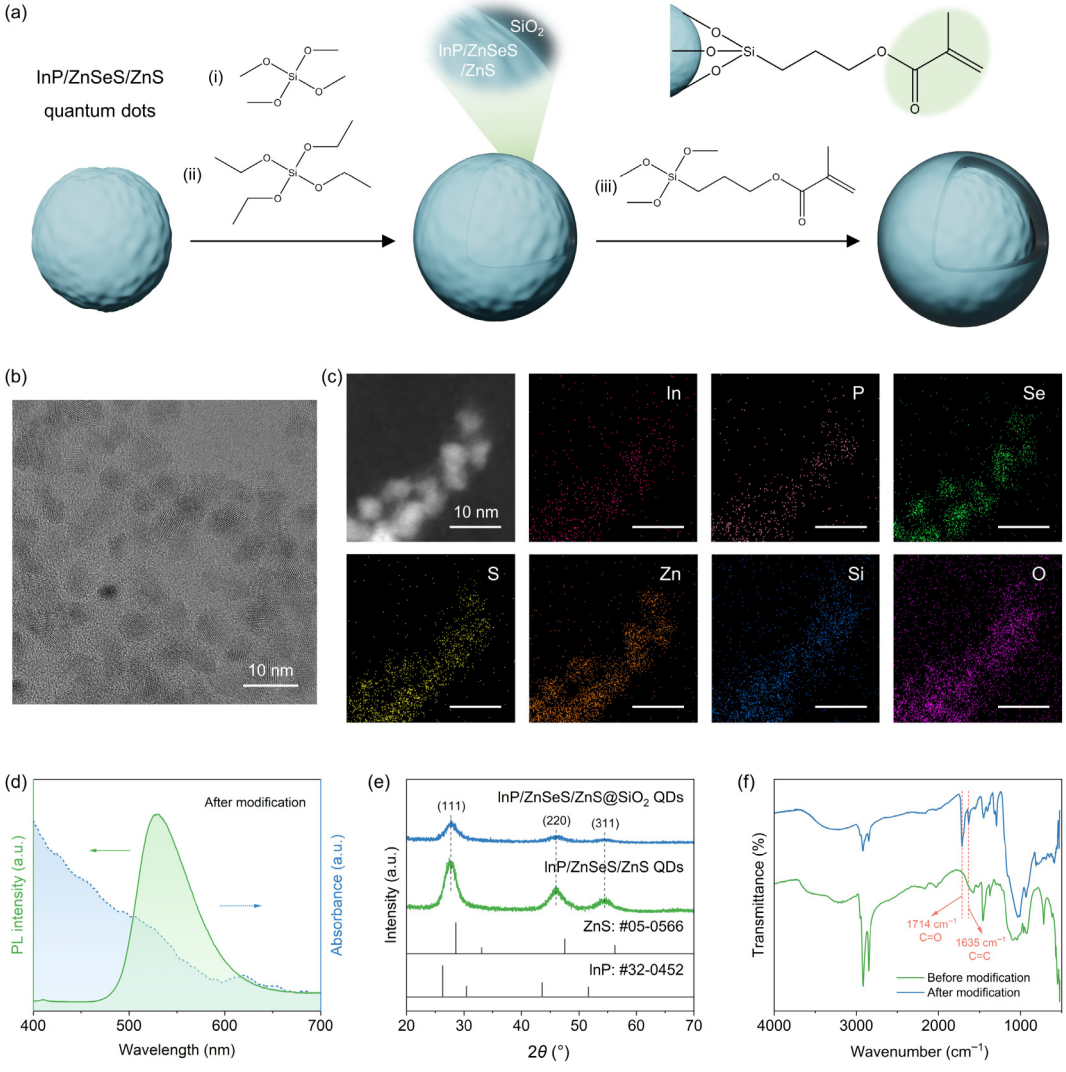

Figure 1 Synthesis and characterization of polymerizable lnP-based QDs. (a) Schematic illustration of synthesizing polymerizable lnP-based QDs. (b) FE-HRTEM image of polymerizable InP/ZnSeS/ZnS QDs. (c) EDS elemental mapping images of as-synthesized QDs. (d) PL spectrum of the polymerizable QDs under 365 nm excitation, alongside corresponding UV–vis absorption spectrum. (e) and (f) XRD patterns and FTIR spectra of QDs before and after modification.

hydrolyzing 3-(trimethoxysilyl)propyl methacrylate (TMSPMA) in the n-hexane solution, we successfully grafted polymerizable methacrylate groups onto the surface of the lnP-based QDs@SiO_2, facilitating their integration into the CLC matrix.

We utilized field emission high resolution transmission electron microscopy (FE-HRTEM) to examine the microstructure of the modified InP-based QDs@SiO_2, revealing uniform QDs with an average diameter of approximately 5 nm (Fig. 1(b) and Fig. S3 in the ESM). Energy-dispersive X-ray spectroscopy (EDS) elemental mapping confirmed the homogeneous distribution of InP/ZnSeS/ZnS QDs within the SiO_2 shell (Fig. 1(c)). Photoluminescence (PL) and ultraviolet–visible (UV–vis) absorption spectra of the modified QDs showed a green emission peak at 528 nm (Fig. 1(d)), slightly red-shifted compared to the emission peak of the unmodified QDs at 521 nm (Fig. S4 in the ESM), which is likely attributed to increased reabsorption caused by QDs within the SiO_2 shell. As can be seen in the X-ray diffraction (XRD) analysis (Fig. 1(e)), the original InP/ZnSeS/ZnS QDs exhibited three broad diffraction peaks corresponding to the (111), (220), and (311) crystal faces of the sample. After modifying with SiO_2 and subsequent surface functionalization, these three diffraction peaks were retained in the InP-based QDs@SiO_2, indicating that the polymerizable InP-based QDs maintained their original crystal structure and phase stability after modification. Furthermore, Fourier-transform infrared (FTIR) spectroscopy revealed the appearance of a new peak at 1714 cm^{-1}, corresponding to C=O groups, and a peak at 1635 cm^{-1}, attributed to C=C bonds [33], confirming the successful grafting of polymerizable functional groups onto the surface of the QDs (Fig. 1(f)).

To obtain high-quality optical chirality, we developed a helical structure-based CLC polymer template to subsequently react with polymerizable QDs, obtaining a homogeneous CPL-active film. We selected the reactive mesogen RM257 as the polymerizable monomer, which underwent cross-linking to form a polymer network in the presence of the photo-initiator I-651 under UV irradiation (Fig. 2(a)) [34]. The chiral dopant R/S5011, possessing a high helical twisting power, was used to induce the self-assembly of the liquid crystal monomers into right-handed or left-handed helical structures (Fig. 2(b)). The obtained CLC polymer template exhibits a periodic helical arrangement, resulting in a photonic bandgap (PBG) that selectively reflects circularly polarized light of the same handedness while transmitting light with the opposite handedness (Fig. 2(c)).

As shown in the transmission spectra in Fig. 2(d), the PBG of the

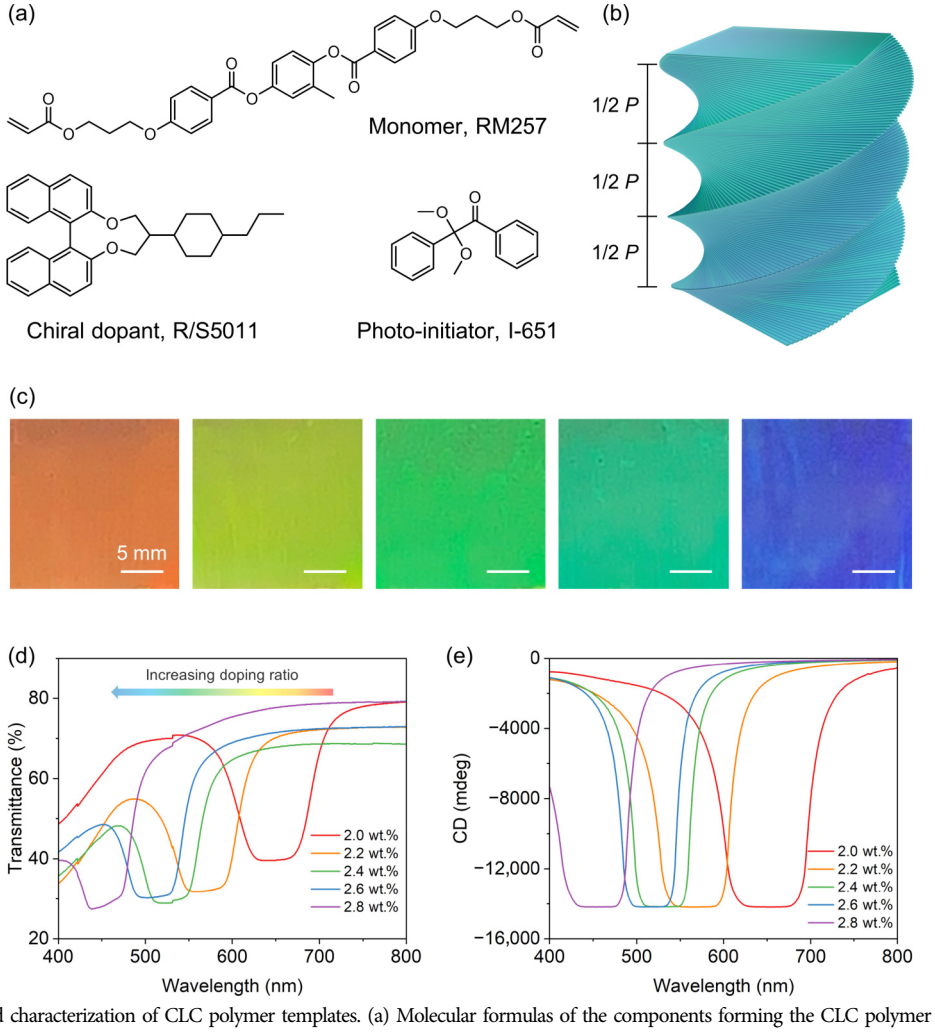

Figure 2 Preparation and characterization of CLC polymer templates. (a) Molecular formulas of the components forming the CLC polymer templates, including the monomer (RM257), chiral dopant (R/S5011), and photo-initiator (I-651). (b) Diagram illustrating the helical structure of the CLC polymer template. (c) Photographs showing circularly polarized structural colors caused by selective reflection of the synthesized templates under natural light. The concentrations of chiral dopant R5011 were 2.0 wt.%, 2.2 wt.%, 2.4 wt.%, 2.6 wt.%, and 2.8 wt.% from left to right, respectively. (d) Transmission spectra and (e) CD spectra corresponding to the templates in (c), illustrating the optical properties across varying doping levels.

CLC polymer template shifted from red to blue by increasing the concentration of the chiral dopants, enabling full coverage of the visible spectrum. This shift is attributed to the decrease in helical pitch caused by the higher concentration of the chiral dopants. Circular dichroism (CD) spectra demonstrated that the CLC polymer templates exhibited high chiral optical activity, with a maximum dissymmetry factor of up to 1.8, approaching the theoretical optimal value of 2 (Fig. 2(e) and Fig. S5 in the ESM). These results highlight the superior performance of the CLC templates we developed.

To achieve stable and uniform dispersion of QDs within the CLC polymer templates, we elaborately designed an *in-situ* helical co-assembly polymerization strategy. This approach involved the covalent anchoring of polymerizable QDs to the CLC polymer templates through UV-initiated free radical polymerization, resulting in the formation of robust covalent bonds at the interface between the polymerized QDs and the templates. We utilized attenuated total reflection-FTIR spectroscopy (ATR-FTIR) to validate this process (Fig. 3(a)). The results indicated that the characteristic peak at 1635 cm^{-1}, associated with the terminal acrylic groups of the polymerizable InP-based QDs and the CLC prepolymer, disappeared after light-induced polymerization, confirming the completion of the curing reaction. We performed XRD measurements on the PSS films to assess their structural characteristics (Fig. 3(b)). The diffuse peak observed at approximately 21° in the 2θ scan indicated the absence of macroscopic molecular or chain orientation, confirming the presence of a polydomain structure in the PSS films; additionally, no low-angle diffraction features indicative of a smectic phase were observed, suggesting that the PSS films form chiral nematic assemblies [35].

To observe the microstructure of the resulted PSS films, we performed polarized optical microscopy (POM) observations in transmission mode (Fig. 3(c) and Fig. S6 in the ESM). The results revealed characteristic oil streaks texture belonging to CLC, confirming the formation of a planar superhelical arrangement [36]. Cross-sectional scanning electron microscopy (SEM) images of the PSS films clearly displayed a periodic layered structure, indicating that the co-assembly with QDs did not disrupt the assembly integrity of the CLC polymer template (Fig. 3(d) and Fig. S7 in the ESM). Additionally, the image revealed a pitch of approximately 320 nm, which, according to Bragg's law ($\lambda = np$), corresponded to selective reflection (i.e., PBG) within the visible spectrum, thereby benefiting the CD and CPL performance of the PSS film. Furthermore, atomic force microscopy (AFM) revealed the presence of a periodic helical arrangement on the surface of the polymerized film (Fig. 3(e) and Fig. S8 in the ESM). Figure 3(f) illustrates the three-dimensional periodic structure characterized by AFM, providing strong evidence for the periodic helical self-assembly of the PSS. The chiral periodic morphology observed in AFM and SEM contributed to the strong CD and CPL signals. We also assessed the fluorescence emission properties of the PSS film (Fig. S9 in the ESM); the film exhibited bright and uniform luminescence under UV irradiation, indicating that the introduction of the CLC polymer templates did not adversely affect the luminescence of the QDs within the composite film. These features are essential for achieving efficient CPL materials with high g_{lum} values.

We further characterized the chiroptical properties of the PSS films (Fig. 4(a)). The CD spectra revealed that the sample doped with S5011 exhibited a positive CD signal (Figs. 4(b) and 4(c)), indicating that the self-assembled helical structure was left-handed. In contrast, the sample doped with R5011 exhibited the opposite behavior. Both left- and right-handed films showed broad CD

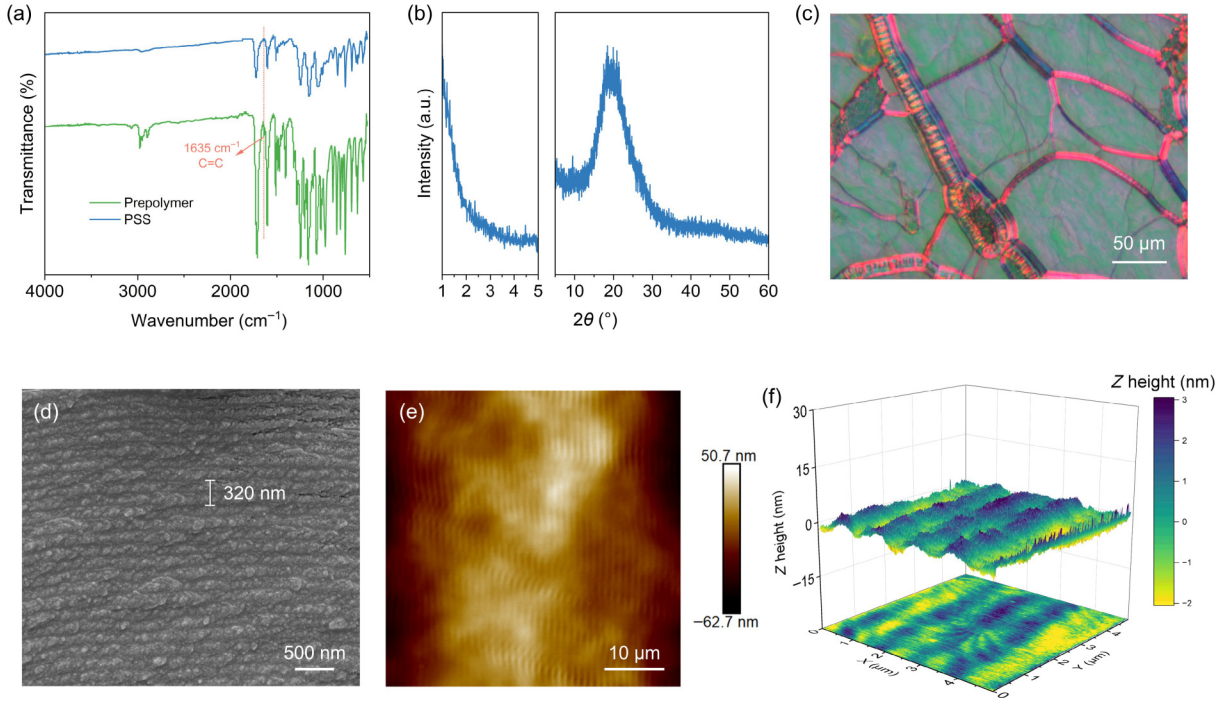

Figure 3 Structural characterization of PSS films. (a) FTIR spectra of the prepolymer and PSS films, highlighting the peak at 1635 cm^{-1} corresponding to the carbon-carbon double bond. (b) XRD pattern of the PSS film including the low- and high-angle regions. (c) POM image of the right-handed PSS film. (d) Cross-sectional SEM image of the right-handed PSS films, showing the periodic arrangement. (e) AFM image of the PSS film surface and (f) locally magnified 3D AFM image, along with its corresponding *Z*-height profile, showing detailed surface topography.

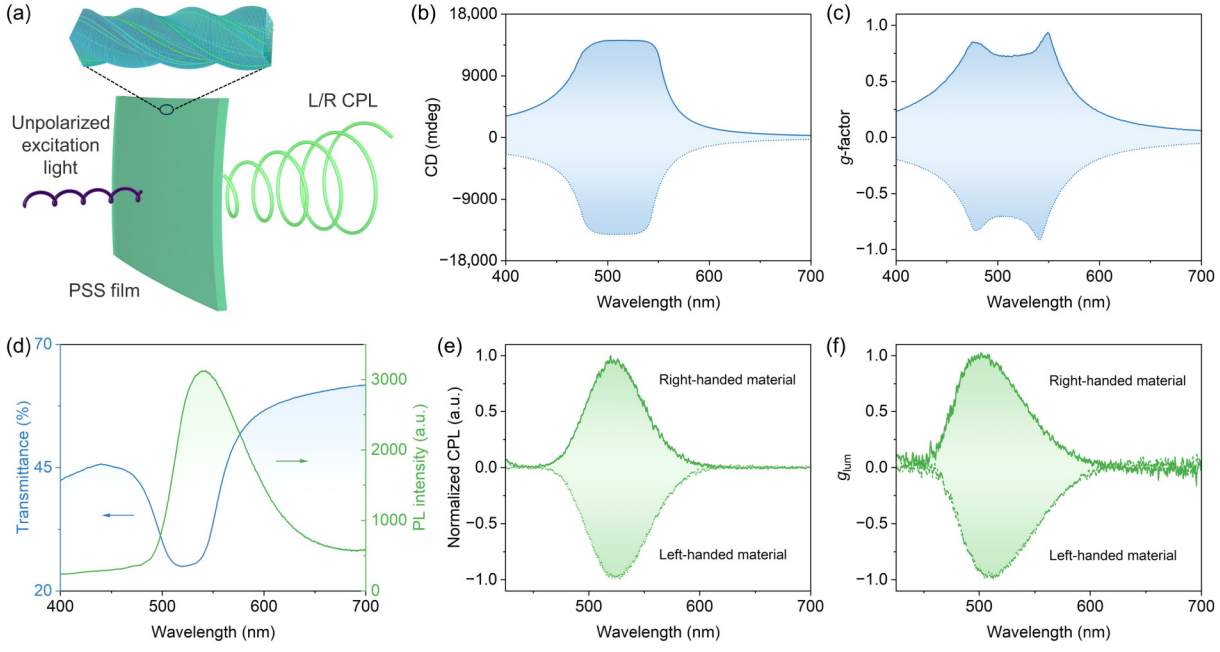

Figure 4 Chiral optical properties of PSS films. (a) Schematic illustration of the transformation of unpolarized excitation light to left- and right-handed circular polarized light. (b) CD spectra, and (c) corresponding *g*-factor values of the left- and right-handed PSS films. (d) Transmission and photoluminescence spectra of the PSS film. (e) CPL spectra and (f) corresponding g_{lum} values of the left- and right-handed PSS films.

bands in the 480–540 nm range, almost consistent with their absorption peaks (Fig. S10 in the ESM).

To achieve optimal CPL performance of the PSS films, the concentration of the chiral dopant was adjusted so that the PBG of the CLC polymer template overlapped with the fluorescence emission band of the polymerizable InP-based QDs (Fig. 4(d)). Furthermore, we evaluated the CPL performance of the PSS films, as shown in Figs. 4(e) and 4(f), which presented the CPL spectra and corresponding g_{lum} curves for samples with different handedness. All films exhibited g_{lum} values of up to 1.0, fully satisfying practical application requirements [37]. For instance, in the case of right-handed PSS, the right-handed CLC polymer template inhibited the propagation of right-handed CPL while promoting the transmission of left-handed CPL, resulting in a strong left-handed CPL signal. To further verify its uniformity on CPL generation, we performed CPL characterization on nine randomly selected regions of the same PSS film. These results indicated an average g_{lum} value of 1.03 ± 0.03, verifying its uniformity on CPL generation (Fig. S11 in the ESM).

To further validate the feasibility of the synthesized strategy and to explore the mechanism of CPL generation and amplification, we prepared two sets of samples: The first group utilized our synthesized PSS films, while the second group employed a physical stacking structure of InP-based QDs and CLC polymer templates. We conducted front- and back-side CPL spectra measurements on both sets of samples to distinguish their unique characteristics. As shown in Figs. 5(a)–5(c) and Fig. S12 in the ESM, for instance, the front and back sides of the left-handed PSS films both exhibited negative CPL signals, indicating the generation of right-handed CPL, with g_{lum} values up to 1.0 in both directions. In contrast, for Sample 2, when the excitation light first passed through the QD layer and then through the right-handed CLC template, a strong left-handed CPL signal was observed (Figs. 5(d)–5(f) and Fig. S13 in the ESM). However, when the excitation light first passed through the right-handed CLC template and then through the QD layer, the CPL signal reversed and significantly weakened. This reversal is likely due to the detector capturing the right-handed circularly polarized light selectively reflected by the CLC template in this configuration. These results demonstrate that the synthesized homogeneous PSS films display high CPL performance, independent of the observation direction. Consequently, the CPL and g_{lum} amplification in this work can be attributed to a photon-resonance effect [16, 30, 38]. This confirms that employing CLC polymer templates with polymerizable QDs is an effective strategy for producing high-quality CPL materials.

Lastly, we demonstrated a potential application. The uniform PSS film can easily achieve graphic displays, which is essential for information security applications. The film can be readily processed into customized emission patterns as needed through a mold. Under daylight, these patterns exhibited inherent structural color, while displaying bright CPL under UV light after incorporating green-emitting QDs. When viewed through different circular polarizers, the left- and right-handed fluorescent emission patterns exhibited marked contrasts, indicating the potential of these patterns for advanced information security labels (Fig. S14 in the ESM).

3 Conclusions

In summary, through the designed *in-situ* helical co-assembly polymerization strategy, we successfully fabricated homogeneous PSS films, addressing challenges related to QD phase separation, stability, and dispersion within CLC matrices. By modifying the QDs with methacrylate groups via SiO_2 encapsulation, we achieved QDs with polymerizable reactivity. With tuning chiral dopants ratio in reactive mesogenic units, we obtained CLC polymer templates with tunable full-spectrum structural color and strong chiroptical activity. The co-polymerization of reactive QDs with the terminal acrylate groups of the CLC polymer templates resulted in uniform solid-state CPL films with a high g_{lum} value of up to 1.0. This strategy provides a novel approach for designing and fabricating

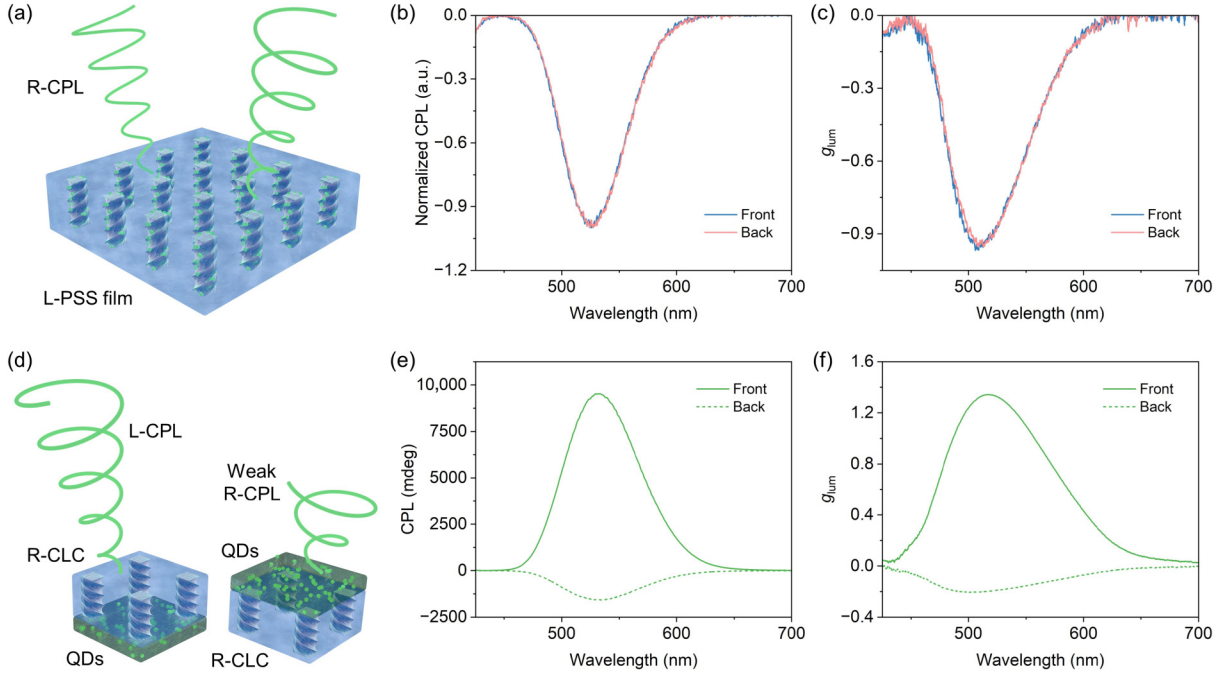

Figure 5 Comparison with physical stacking structure. (a) Schematic illustrating the right-handed CPL from homogeneous left-handed PSS films. (b) CPL spectra, and (c) corresponding g_{lum} values of the left-handed PSS film, measured from the front and back sides. (d) Schematic diagram of the physical stacking structures, showing configurations of QDs/R-CLC and R-CLC/QDs. (e) CPL spectra and (f) corresponding g_{lum} values of the QDs/R-CLC and R-CLC/QDs stacks, measured from the front and back sides.

high-performance CPL materials, with potential applications in information security, advanced displays, quantum computing, and beyond.

4 Experimental

4.1 Chemicals

InI_3 (99.999%) was purchased from Alfa Aesar. Trioctylphosphine (TOP, > 97%), $ZnBr_2$ (98%), 1-octadecene (ODE, 90%), tris (dimethylamino)phosphine ($(DMA)_3P$, 98%), 1-dodecanethiol (DDT, 98%), and oleylamine (OAm, 90%) were purchased from Adamas. Zinc stearate ($Zn(St)_2$, 77.69%–93.23%), sulfur powder (≥ 99.99%), and selenium powder (≥ 99.999%) were purchased from Sigma-Aldrich. TEOS (≥ 99%), TMOS (≥ 98%), and TMSPMA (≥ 97%) were purchased from Aladdin Bio-Chem Technology Co., Ltd. RM257 and chiral dopants (R5011 and S5011) were purchased from the Shijiazhuang Yesheng Chemical Technology Co., Ltd. All liquid crystal cells with a 25 μm cell gap were homemade. All chemicals were used directly without any further purification.

4.2 Synthesis of InP/ZnSeS/ZnS QDs

First, 0.5055 g of InI_3, 1.4865 g of $ZnBr_2$ (molar ratio of In/Zn = 1:6.5), and 15.0 mL of OAm were mixed in a three-neck flask. The solution was then heated to 120 °C at a rate of 10 °C·min^{-1} and degassed for 20 min. The mixture was subsequently heated to 200 °C, after which 7.2 mmol of $(DMA)_3P$ was added. After maintaining this temperature for 6 min, 36 mL of zinc precursor solution (9.0 g of $Zn(St)_2$ dissolved in 36.0 mL of ODE) , along with 3.6 mmol (1.1 M) TOP/(Se+S) was rapidly injected into the reaction mixture. The solution was then heated to 260 °C and maintained at this temperature for 120 min. Finally, 4.5 mL DDT was injected into the solution at 280 °C and kept for 1 h. After the reaction was complete, the mixture was naturally cooled down to room temperature. The products were then isolated by centrifugation, washed with ethanol three times, and resuspended in hexane for further use.

4.3 Synthesis of polymerizable QDs

A solution of 20 mL QDs (0.64 mg/mL) in hexane was prepared, followed by the addition of 100 μL of TMOS under continuous stirring at room temperature for 1 h. Subsequently, 300 μL of TEOS was introduced into the mixture, with 100 μL added every hour over a period of 3 h. The resulting solution was then mixed with ethanol in the volume ratio of 1:3 and centrifuged at 9000 rpm for 10 min. Upon removal of the supernatant, the precipitate was then redispersed in 20 mL hexane. Next, 200 μL of TMSPMA was added to the prepared solution, which was then stirred continuously at 60 °C and refluxed under a nitrogen atmosphere for 10 h. After the reaction was completed, the resulting precipitate was washed twice with hexane and ethanol. After each wash, the solution was centrifuged at 9000 rpm for 10 min. Finally, the product was dried overnight in an oven at 45 °C.

4.4 Fabrication of PSS films

First, we prepared left- and right-handed CLCs by combining RM257 with the chiral dopants S5011 and R5011, respectively. To tune the PBG of the CLCs to align with the red, green, and blue spectral regions, chiral dopants were added at weight ratios of 2.0 wt.%, 2.4 wt.%, and 2.8 wt.%.

Next, the precursor was prepared by combining 95.0 wt.% of a mixture of CLCs and chiral dopants, 1.0 wt.% of I-651, and 4.0 wt.% of polymerizable QDs powder. The mixture was then heated to 120 °C to ensure uniformity, followed by gradual cooling to 90 °C. At this temperature, the solution was injected into liquid crystal cells through capillary action. Polymerization was

subsequently carried out under UV light at 90 °C for 30 min. Afterward, the CLC film could be easily peeled off from the liquid crystal cell.

4.5 Characterization

CD and CPL spectra were measured on JASCO J-1500 spectrophotometer and JASCO CPL-300 spectrophotometer, respectively. Reflectance spectra were measured with an ultraviolet/visible/near infrared spectrometer (SolidSpec-3700i DUV). Fluorescence spectra were measured with a fluorescence spectrometer (Hitachi, F-4700). X-ray diffraction patterns were measured on a diffractometer (X'Pert PRO MPD) with Cu Kα radiation (wavelength: λ = 1.54178 Å). QDs dispersed in hexane were drop-cast on carbon-supported Cu grids for TEM and FE-HRTEM analysis, which was performed on JEM-2100Plus and JEM-F200 microscopies with acceleration voltages of 200 kV. The FTIR spectrum was measured with an FTIR microscopy (Nicolet iN10MX). Scanning electron microscopy images were obtained using a field emission scanning electron microscopy (Zeiss Supra 40, at an acceleration voltage of 3.0 kV). POM images were recorded on an upright materials microscopy (Mshot MP41).

Electronic Supplementary Material: Supplementary material (TEM images, FE-HRTEM images, EDS elemental mapping images, PL spectra, UV–vis absorption spectra, POM images, SEM images, AFM images, and CPL spectra) is available in the online version of this article at https://doi.org/10.26599/NR.2025.94907150.

Data availability

All data needed to support the conclusions in the paper are presented in the manuscript and the Electronic Supplementary Material. Additional data related to this paper may be requested from the corresponding author upon request.

Acknowledgements

This work was supported by the National Key Research and Development Program of China (No. 2021YFA1500400), the National Natural Science Foundation of China (Nos. 22071226, 22471253, and 224B2116), the Hundred Talent Program of the Chinese Academy of Sciences (No. KJ2060007002), the Collaborative Innovation Program of Hefei Science Center, Chinese Academy of Sciences (Nos. CX2060000017 and 2022HSC-CIP016), the Anhui Provincial Natural Science Foundation, China (No. BJ2060190120), the College Student Research Program (No. WW0000000888), and the Funding of University of Science and Technology of China (Nos. KY2060000168, YD2060002013, and KY2060000198). This work was partially carried out at the USTC Center for Micro and Nanoscale Research and Fabrication, and we thank Dr. Yaping Li for help on micro/nano fabrication and characterization.

Declaration of competing interest

All the contributing authors report no conflict of interests in this work.

Author contribution statement

M. J. Z.: Data curation, writing manuscript, experimental design, collecting data. W. T. G.: Experimental design, conducting experiments, collecting data. S. S. Z.: Data curation, validation. T. T. Z.: Project administration, data curation, funding acquisition, revising manuscript. All the authors have approved the final manuscript.

Use of AI statement

None.

References

[1] Zhang, M. J.; Guo, Q.; Li, Z. Y.; Zhou, Y. J.; Zhao, S. S.; Tong, Z.; Wang, Y. X.; Li, G. G.; Jin, S.; Zhu, M. Z. et al. Processable circularly polarized luminescence material enables flexible stereoscopic 3D imaging. *Sci. Adv.* **2023**, *9*, eadi9944.

[2] Zhan, X. Q.; Xu, F. F.; Zhou, Z. H.; Yan, Y. L.; Yao, J. N.; Zhao, Y. S. 3D laser displays based on circularly polarized lasing from cholesteric liquid crystal arrays. *Adv. Mater.* **2021**, *33*, 2104418.

[3] Yang, X. F.; Gao, X. Q.; Zheng, Y. X.; Kuang, H.; Chen, C. F.; Liu, M. H.; Duan, P. F.; Tang, Z. Y. Recent progress of circularly polarized luminescence materials from Chinese perspectives. *CCS Chem.* **2023**, *5*, 2760–2789.

[4] Gong, Z. L.; Zhu, X. F.; Zhou, Z. H.; Zhang, S. W.; Yang, D.; Zhao, B.; Zhang, Y. P.; Deng, J. P.; Cheng, Y. X.; Zheng, Y. X. et al. Frontiers in circularly polarized luminescence: Molecular design, self-assembly, nanomaterials, and applications. *Sci. China Chem.* **2021**, *64*, 2060–2104.

[5] Cai, J. R.; Zhang, W.; Xu, L. G.; Hao, C. L.; Ma, W.; Sun, M. Z.; Wu, X. L.; Qin, X.; Colombari, F. M.; De Moura, A. F. et al. Polarization-sensitive optoionic membranes from chiral plasmonic nanoparticles. *Nat. Nanotechnol.* **2022**, *17*, 408–416.

[6] Shi, B. M.; Qu, A. H.; Li, Z. D.; Xiong, Y. C.; Ji, J. J.; Xu, L. G.; Xu, C. L.; Sun, M. Z.; Kuang, H. Chiral intranasal nanovaccines as antivirals for respiratory syncytial virus. *Adv. Mater.* **2024**, *36*, e2408090.

[7] Xu, L. G.; Wang, X. X.; Wang, W. W.; Sun, M. Z.; Choi, W. J.; Kim, J. Y.; Hao, C. L.; Li, S.; Qu, A. H.; Lu, M. R. et al. Enantiomer-dependent immunological response to chiral nanoparticles. *Nature* **2022**, *601*, 366–373.

[8] Liu, J.; Wu, J. J.; Wei, J.; Huang, Z. J.; Zhou, X. Y.; Bao, J. Y.; Lan, R. C.; Ma, Y.; Li, B. X.; Yang, H. et al. Dynamically modulating the dissymmetry factor of circularly polarized organic ultralong room-temperature phosphorescence from soft helical superstructures. *Angew. Chem., Int. Ed.* **2024**, *63*, e202319536.

[9] Wang, X. J.; Zhao, B.; Deng, J. P. Liquid crystals doped with chiral fluorescent polymer: Multi-color circularly polarized fluorescence and room-temperature phosphorescence with high dissymmetry factor and anti-counterfeiting application. *Adv. Mater.* **2023**, *35*, 2304405.

[10] Yi, C. L.; Liu, H.; Zhang, S. Y.; Yang, Y. Q.; Zhang, Y.; Lu, Z. Y.; Kumacheva, E.; Nie, Z. H. Self-limiting directional nanoparticle bonding governed by reaction stoichiometry. *Science* **2020**, *369*, 1369–1374.

[11] Liu, Y. Z.; Gao, X. B.; Zhao, B.; Deng, J. P. Circularly polarized luminescence in quantum dot-based materials. *Nanoscale* **2024**, *16*, 6853–6875.

[12] Jiang, Y. Z.; Sun, C. J.; Xu, J.; Li, S. S.; Cui, M. H.; Fu, X. L.; Liu, Y.; Liu, Y. Q.; Wan, H. Y.; Wei, K. Y. et al. Synthesis-on-substrate of quantum dot solids. *Nature* **2022**, *612*, 679–684.

[13] Chen, Q. L.; Ding, Z. J.; Zhang, L.; Wang, D.; Geng, C.; Feng, Y. X.; Zhang, J.; Ren, M.; Li, S. S.; Qaid, S. M. H. et al. Uniaxial-oriented chiral perovskite for flexible full-stokes polarimeter. *Adv. Mater.* **2024**, *36*, 2400493.

[14] Liu, P.; Lou, Y. J.; Ding, S. H.; Zhang, W. D.; Wu, Z. H.; Yang, H. C.; Xu, B.; Wang, K.; Sun, X. W. Green InP/ZnSeS/ZnS core multi-

shelled quantum dots synthesized with aminophosphine for effective display applications. *Adv. Funct. Mater.* **2021**, *31*, 2008453.
[15] Zhang, X.; Xu, Y. Y.; Valenzuela, C.; Zhang, X. F.; Wang, L.; Feng, W.; Li, Q. Liquid crystal-templated chiral nanomaterials: From chiral plasmonics to circularly polarized luminescence. *Light: Sci. Appl.* **2022**, *11*, 223.
[16] Wu, Y.; Li, M. Q.; Zheng, Z. G.; Yu, Z. Q.; Zhu, W. H. Liquid crystal assembly for ultra-dissymmetric circularly polarized luminescence and beyond. *J. Am. Chem. Soc.* **2023**, *145*, 12951–12966.
[17] Yang, X. K.; Lv, J. W.; Zhang, J.; Shen, T. X.; Xing, T. X.; Qi, F. L.; Ma, S. H.; Gao, X. Q.; Zhang, W.; Tang, Z. Y. Tunable circularly polarized luminescence from inorganic chiral photonic crystals doped with quantum dots. *Angew. Chem., Int. Ed.* **2022**, *61*, e202201674.
[18] Liu, J.; Song, Z. P.; Wei, J.; Wu, J. J.; Wang, M. Z.; Li, J. G.; Ma, Y.; Li, B. X.; Lu, Y. Q.; Zhao, Q. Circularly polarized organic ultralong room-temperature phosphorescence with a high dissymmetry factor in chiral helical superstructures. *Adv. Mater.* **2024**, *36*, 2306834.
[19] Wang, H. Q.; Tang, Y. Q.; Huang, Z. Y.; Wang, F. Z.; Qiu, P. F.; Zhang, X. F.; Li, C. H.; Li, Q. A dual-responsive liquid crystal elastomer for multi-level encryption and transient information display. *Angew. Chem., Int. Ed.* **2023**, *62*, e202313728.
[20] Fan, Q. Y.; Li, Z. Y.; Jiang, K. D.; Gao, J. J.; Lin, S. Y.; Guo, J. B. Tunable circular polarization room temperature phosphorescence with ultrahigh dissymmetric factor by cholesteric liquid crystal elastomers. *Cell Rep. Phys. Sci.* **2023**, *4*, 101583.
[21] Zheng, Z. G.; Hu, H. L.; Zhang, Z. P.; Liu, B. H.; Li, M. Q.; Qu, D. H.; Tian, H.; Zhu, W. H.; Feringa, B. L. Digital photoprogramming of liquid-crystal superstructures featuring intrinsic chiral photoswitches. *Nat. Photonics* **2022**, *16*, 226–234.
[22] Chen, G. D.; Pei, H. W.; Zhang, X. F.; Shi, W.; Liu, M. J.; Faul, C. F. J.; Yang, B.; Zhao, Y.; Liu, K.; Lu, Z. Y. et al. Liquid-crystalline behavior on dumbbell-shaped colloids and the observation of chiral blue phases. *Nat. Commun.* **2022**, *13*, 5549.
[23] Hu, H. L.; Liu, B. H.; Li, M. Q.; Zheng, Z. G.; Zhu, W. H. A quadri-dimensional manipulable laser with an intrinsic chiral photoswitch. *Adv. Mater.* **2022**, *34*, 2110170.
[24] Shi, Y. H.; Han, J. L.; Li, C. X.; Zhao, T. H.; Jin, X.; Duan, P. F. Recyclable soft photonic crystal film with overall improved circularly polarized luminescence. *Nat. Commun.* **2023**, *14*, 6123.
[25] Zhou, Y. J.; Wang, Y. X.; Song, Y. H.; Zhao, S. S.; Zhang, M. J.; Li, G. G.; Guo, Q.; Tong, Z.; Li, Z. Y.; Jin, S. et al. Helical-caging enables single-emitted large asymmetric full-color circularly polarized luminescence. *Nat. Commun.* **2024**, *15*, 251.
[26] Guo, Q.; Zhang, M. J.; Tong, Z.; Zhao, S. S.; Zhou, Y. J.; Wang, Y. X.; Jin, S.; Zhang, J.; Yao, H. B.; Zhu, M. Z. et al. Multimodal-responsive circularly polarized luminescence security materials. *J. Am. Chem. Soc.* **2023**, *145*, 4246–4253.
[27] Bagchi, K.; Emeršič, T.; Martínez-González, J. A.; De Pablo, J. J.; Nealey, P. F. Functional soft materials from blue phase liquid crystals. *Sci. Adv.* **2023**, *9*, eadh9393.
[28] Kang, W. X.; Tang, Y. Q.; Meng, X. Y.; Lin, S. Y.; Zhang, X. F.; Guo, J. B.; Li, Q. A photo- and thermo-driven azoarene-based circularly polarized luminescence molecular switch in a liquid crystal host. *Angew. Chem., Int. Ed.* **2023**, *62*, e202311486.
[29] Liu, S. J.; Liu, X.; Wu, Y. Z.; Zhang, D. W.; Wu, Y.; Tian, H.; Zheng, Z. G.; Zhu, W. H. Circularly polarized perovskite luminescence with dissymmetry factor up to 1.9 by soft helix bilayer device. *Matter* **2022**, *5*, 2319–2333.
[30] Zhang, X.; Li, L.; Chen, Y. H.; Valenzuela, C.; Liu, Y.; Yang, Y. Z.; Feng, Y. F.; Wang, L.; Feng, W. Mechanically tunable circularly polarized luminescence of liquid crystal-templated chiral perovskite quantum dots. *Angew. Chem., Int. Ed.* **2024**, *63*, e202404202.
[31] Shen, X. X.; He, H. B.; Zheng, D.; Cao, W.; Sang, Y. T.; Nie, Z. H. Engineering the electrostatic interactions between oppositely charged polymer-grafted nanoparticles for constructing colloid molecules on substrates. *ACS Nano* **2024**, *18*, 20999–21008.
[32] Huang, S. Q.; Li, Z. C.; Kong, L.; Zhu, N. W.; Shan, A. D.; Li, L. Enhancing the stability of $CH_3NH_3PbBr_3$ quantum dots by embedding in silica spheres derived from tetramethyl orthosilicate in "waterless" toluene. *J. Am. Chem. Soc.* **2016**, *138*, 5749–5752.
[33] Yang, X.; Valenzuela, C.; Zhang, X.; Chen, Y. H.; Yang, Y. Z.; Wang, L.; Feng, W. Robust integration of polymerizable perovskite quantum dots with responsive polymers enables 4D-printed self-deployable information display. *Matter* **2023**, *6*, 1278–1294.
[34] Choi, S. H.; Kim, J. H.; Ahn, J.; Kim, T.; Jung, Y.; Won, D.; Bang, J.; Pyun, K. R.; Jeong, S.; Kim, H. et al. Phase patterning of liquid crystal elastomers by laser-induced dynamic crosslinking. *Nat. Mater.* **2024**, *23*, 834–843.
[35] Yin, L.; Miao, T. F.; Cheng, X. X.; Jiang, Z. C.; Tong, X.; Zhang, W.; Zhao, Y. Chiral liquid crystalline elastomer for twisting motion without preset alignment of mesogens. *ACS Macro Lett.* **2021**, *10*, 690–696.
[36] Shi, Y. H.; Han, J. L.; Jin, X.; Miao, W. G.; Zhang, Y.; Duan, P. F. Chiral luminescent liquid crystal with multi-state-reversibility: Breakthrough in advanced anti-counterfeiting materials. *Adv. Sci.* **2022**, *9*, 2201565.
[37] Zhang, C.; Zhao, S.; Zhang, M. M.; Li, B.; Dong, X. Y.; Zang, S. Q. Emergent induced circularly polarized luminescence in host-guest crystalline porous assemblies. *Coord. Chem. Rev.* **2024**, *514*, 215859.
[38] Li, M. Q.; Hu, H. L.; Liu, B. H.; Liu, X.; Zheng, Z. G.; Tian, H.; Zhu, W. H. Light-reconfiguring inhomogeneous soft helical pitch with fatigue resistance and reversibility. *J. Am. Chem. Soc.* **2022**, *144*, 20773–20784.